# New $\beta$-decaying state in $^{214}$Bi

B. Andel,[1,2,*] P. Van Duppen,[1] A. N. Andreyev,[3,4] A. Blazhev,[5] H. Grawe,[6,†] R. Lică,[7] H. Naïdja,[8] M. Stryjczyk,[1,9] A. Algora,[10,11] S. Antalic,[2] A. Barzakh,[12] J. Benito,[13] G. Benzoni,[14] T. Berry,[15] M. J. G. Borge,[16] K. Chrysalidis,[17] C. Clisu,[7] C. Costache,[7] J. G. Cubiss,[3] H. De Witte,[1] D. V. Fedorov,[12] V. N. Fedosseev,[17] L. M. Fraile,[13] H. O. U. Fynbo,[18] P. T. Greenlees,[9] L. J. Harkness-Brennan,[19] M. Huyse,[1] A. Illana,[20] J. Jolie,[5] D. S. Judson,[19] J. Konki,[9] I. Lazarus,[21] M. Madurga,[17] N. Marginean,[7] R. Marginean,[7] C. Mihai,[7] B. A. Marsh,[17] P. Molkanov,[12] P. Mosat,[2] J. R. Murias,[13,22] E. Nacher,[10] A. Negret,[7] R. D. Page,[19] S. Pascu,[7] A. Perea,[16] V. Pucknell,[21] P. Rahkila,[9] E. Rapisarda,[17] K. Rezynkina,[1,23] V. Sánchez-Tembleque,[13] K. Schomacker,[5] M. D. Seliverstov,[12] C. Sotty,[7] L. Stan,[7] C. Sürder,[24] O. Tengblad,[16] V. Vedia,[13] S. Viñals,[16] R. Wadsworth,[3] and N. Warr[5]

(IDS Collaboration)

[1]*KU Leuven, Instituut voor Kern- en Stralingsfysica, B-3001 Leuven, Belgium*
[2]*Department of Nuclear Physics and Biophysics, Comenius University in Bratislava, 84248 Bratislava, Slovakia*
[3]*Department of Physics, University of York, York YO10 5DD, United Kingdom*
[4]*Advanced Science Research Center, Japan Atomic Energy Agency, Tokai-mura, Ibaraki 319-1195, Japan*
[5]*Institut für Kernphysik, Universität zu Köln, 50937 Köln, Germany*
[6]*GSI Helmholtzzentrum für Schwerionenforschung, GmbH, 64291 Darmstadt, Germany*
[7]*"Horia Hulubei" National Institute for R & D in Physics and Nuclear Engineering, RO-077125 Bucharest, Romania*
[8]*Laboratoire de Physique Mathematique et Subatomique, Université Constantine 1, Constantine 25000, Algeria*
[9]*University of Jyväskylä, Department of Physics, P.O. Box 35, FI-40014 Jyväskylä, Finland*
[10]*Instituto de Física Corpuscular, CSIC - Universidad de Valencia, E-46980 Valencia, Spain*
[11]*Institute of Nuclear Research (ATOMKI), P.O.Box 51, H-4001 Debrecen, Hungary*
[12]*Petersburg Nuclear Physics Institute, NRC Kurchatov Institute, 188300 Gatchina, Russia*
[13]*Grupo de Física Nuclear, Universidad Complutense de Madrid, 28040 Madrid, Spain*
[14]*Istituto Nazionale di Fisica Nucleare, Sezione di Milano, I-20133 Milano, Italy*
[15]*Department of Physics, University of Surrey, Guildford GU2 7XH, United Kingdom*
[16]*Instituto de Estructura de la Materia, CSIC, Serrano 113 bis, E-28006 Madrid, Spain*
[17]*CERN, CH-1211 Geneve 23, Switzerland*
[18]*Department of Physics and Astronomy, Aarhus University, DK-8000 Aarhus C, Denmark*
[19]*Department of Physics, Oliver Lodge Laboratory, University of Liverpool, Liverpool L69 7ZE, United Kingdom*
[20]*Instituto Nazionale di Fisica Nucleare, Laboratori Nazionali di Legnaro, I-35020 Legnaro, Italy*
[21]*STFC Daresbury, Daresbury, Warrington WA4 4AD, United Kingdom*
[22]*Institut Laue-Langevin, CS 20156, 38042 Grenoble Cedex 9, France*
[23]*Université de Strasbourg, CNRS, IPHC UMR7178, F-67000, Strasbourg, France*
[24]*Institut für Kernphysik, Technische Universität Darmstadt, 64289 Darmstadt, Germany*

(Received 12 July 2021; accepted 21 October 2021; published 2 November 2021)

A new $\beta$-decaying state in $^{214}$Bi has been identified at the ISOLDE Decay Station at the CERN-ISOLDE facility. A preferred $I^\pi = (8^-)$ assignment was suggested for this state based on the $\beta$-decay feeding pattern to levels in $^{214}$Po and shell-model calculations. The half-life of the $I^\pi = (8^-)$ state was deduced to be $T_{1/2} = 9.39(10)$ min. The deexcitation of the levels populated in $^{214}$Po by the $\beta$ decay of this state was investigated via $\gamma$-$\gamma$ coincidences and a number of new levels and transitions was identified. Shell-model calculations for excited states in $^{214}$Bi and $^{214}$Po were performed using two different effective interactions: the H208 and the modified Kuo-Herling particle interaction. Both calculations agree on the interpretation of the new $\beta$-decaying state as an $I^\pi = 8^-$ isomer and allow for tentative assignment of shell-model states to several high-spin states in $^{214}$Po.

DOI: 10.1103/PhysRevC.104.054301

## I. INTRODUCTION

The nuclear structure of the odd-odd, neutron-rich bismuth isotopes with $A \geqslant 210$ provides an excellent testing ground for shell-model calculations. With one proton above the closed shell at $Z = 82$ and neutrons gradually filling orbitals above the closed shell at $N = 126$, the lowest-lying levels have dominant components in the shell-model wave

*boris.andel@fmph.uniba.sk
†Deceased.

functions stemming from the $[\pi 0h_{9/2} \otimes \nu 1g_{9/2}]_{0^-,\ldots,9^-}$ multiplet. Studying this multiplet gives important information on the residual proton-neutron interaction, while the specific ordering of these states gives rise to isomerism. For instance, in the isotopes $^{210}$Bi and $^{212}$Bi, low-lying high-spin isomers with $I^\pi = 9^-$ [1] and $I^\pi = (9^-, 8^-)$ [2], respectively, and low-spin $I^\pi = 1^-$ ground states (g.s.) have been reported [1,2]. The order of the states is to some extent reversed in the heavier isotopes $^{216,218}$Bi. A high-spin, possibly $I^\pi = (6^-, 7^-)$, g.s. was observed in $^{216}$Bi [3] and an $I^\pi = (6^-, 7^-, 8^-)$ g.s. was proposed for $^{218}$Bi [4]. Moreover, a low-spin isomer was identified in $^{216}$Bi [5,6][1] with $I^\pi = (3)$ suggested in the evaluation in Ref. [7].

In $^{214}$Bi, only the $I^\pi = 1^-$ $\beta$-decaying state, presumed to be the g.s., is known [8]. The states in $^{214}$Bi were previously studied via the $\beta^-$ decay of the $I^\pi = 0^+$ g.s. in $^{214}$Pb and via $\alpha$ decay of the $I^\pi = (3^-)$ g.s. of $^{218}$At [8–11]. In these studies, only low-spin states ($I \leqslant 4$) were populated, and thus high-spin levels were inaccessible.

Detailed $\beta$-decay measurements of the $I^\pi = 1^-$ g.s. in $^{214}$Bi were performed over the years and an extensive decay scheme of populated low-spin levels in $^{214}$Po was compiled in the Nuclear Data Sheets (NDS) [8]. A few of the low-spin states in $^{214}$Po are populated also in the $\alpha$ decay of the $I^\pi = 0^+$ g.s. in $^{218}$Rn [8]. However, information on high-spin ($I > 4$) levels in $^{214}$Po is scarce and comes from a single in-beam study [12]. States up to the $12^+$ level at 2734 keV were identified and $I^\pi$ assignments were made for several of these states based on $\gamma$-ray angular distributions [12].

The present study reports on the identification of a new, high-spin $\beta$-decaying state in $^{214}$Bi and on investigation of populated high-spin states in $^{214}$Po.

## II. EXPERIMENT

The experiment was performed at the ISOLDE facility at CERN [13,14]. The isotope $^{214}$Bi was produced in proton-induced spallation reactions in a thick $UC_x$ target (50 g/cm$^2$). A beam of 1.4-GeV protons with an intensity up to 2.1 $\mu$A was provided by the Proton Synchrotron Booster. The proton beam consisted of 2.4-$\mu$s-long pulses with a 1.2-s period, which were grouped into a so-called supercycle containing typically around 30 pulses.

The produced isotopes diffused from the target heated to ≈2300 K and effused via the heated transfer line into a hot cavity, where ionization by the Resonance Ionization Laser Ion Source (RILIS) [15,16] took place. A three-step resonance ionization scheme using laser light with wavelengths of 306.9, 555.4, and 532 nm (the third being nonresonant) [17] was employed to selectively ionize bismuth isotopes. The hyperfine spectrum of $^{214}$Bi was measured in our preceding laser-spectroscopy experiment [18]. In the present experiment, the wavelength of the first-step laser was set to the frequency of specific hyperfine transitions to preferentially ionize the new $\beta$-decaying state in $^{214}$Bi. However, because of the linewidth of ≈12 GHz, the previously known $I^\pi = 1^-$ $\beta$-decaying state in $^{214}$Bi [8] was ionized as well. Based on the numbers of $\gamma$ rays in the singles spectrum in Fig. 1 corrected for absolute $\gamma$-ray intensities and efficiencies (325-keV $\gamma$ ray for the new state and 1120-keV transition for the $I^\pi = 1^-$ state), the numbers of decayed nuclei in the chamber were $N$ (new state)$= 3.15(9) \times 10^7$ and $N(I^\pi = 1^-) = 2.42(7) \times 10^8$. The absolute $\gamma$-ray intensity for decay of the $I^\pi = 1^-$ state was taken from Ref. [8]. Despite higher contribution of the $I^\pi = 1^-$ state, decays of the new state could be resolved and studied using $\gamma$-$\gamma$ coincidences (Secs. III A and III B).

The ions were extracted and accelerated by a 30-kV potential and sent through the High Resolution Separator, where selection according to $A/q = 214$ took place. To suppress isobaric contamination from a surface-ionized, short-lived $^{214}$Fr [$T_{1/2}(^{214}\mathrm{Fr}^g) = 5.5(3)$ ms, $T_{1/2}(^{214}\mathrm{Fr}^m) = 3.38(5)$ ms [8]], the beam gate was closed for the first 100 ms after each proton pulse.

The mass-separated beam was delivered to the ISOLDE Decay Station (IDS) [19] and implanted on an aluminized Mylar tape. Four HPGe Clover detectors for $\gamma$-ray detection and a plastic scintillator for $\beta$-particle detection were placed outside the vacuum chamber in close geometry around the implantation position. The energy calibration of the HPGe detectors was performed with a $^{152}$Eu source, but four crystals (out of 16) were calibrated by using well-known $\gamma$-ray peaks from implanted activity of $^{210}$Rn and $I^\pi = 1^-$ state in $^{214}$Bi [8], because of slight shift in gains. The energy resolution at 1120 keV was 2.6 keV (full width at half maximum). For the absolute detection efficiency calibration, intensity-calibrated sources $^{152}$Eu and $^{133}$Ba were used.

All $\gamma$-ray spectra were created using add-back for all four crystals within each Clover detector. Background subtraction for $\gamma$-$\gamma$ coincidence spectra and for time distribution spectra was done in a standard way by gating on the background on the left-hand side and on the right-hand side of the peak of interest.

## III. RESULTS AND DISCUSSIONS

The identification of the new $\beta$-decaying state in $^{214}$Bi raises a question as to whether the $I^\pi = 1^-$ state in $^{214}$Bi is indeed the ground state, because the relative position of these two states could not be experimentally determined in our study. However, based on the trend in neighboring $^{210,212}$Bi nuclei, supported by the shell-model calculations discussed in Sec. IV A, we refer to the $I^\pi = 1^-$ state as the g.s. ($^{214}$Bi$^g$) and the new $\beta$-decaying state as an isomer ($^{214}$Bi$^m$).

In the singles $\gamma$-ray spectrum shown in Fig. 1, known transitions following the $\beta^-$ decay of $^{214}$Bi$^g$ can be readily identified, for example, the 609- ($2_1^+ \rightarrow 0_1^+$), 1120- ($2_5^+ \rightarrow 2_1^+$), 1238- ($2_6^+ \rightarrow 2_1^+$), 1730- ($2_5^+ \rightarrow 0_1^+$), and 1764-keV ($1_1^+ \rightarrow 0_1^+$) transitions [8]. Moreover, the g.s. band cascade following the deexcitation of the $8_1^+$ level in the daughter nuclide $^{214}$Po, reported in an in-beam study [12], is present as well: the 245- ($8_1^+ \rightarrow 6_1^+$), 325- ($6_1^+ \rightarrow 4_1^+$), and 406-keV ($4_1^+ \rightarrow 2_1^+$) transitions are visible (see the decay scheme in Fig. 2). These four yrast transitions from the cascade below

[1]At the time of the studies [5,6], the g.s. was not yet known, therefore the long-lived state was not discussed as an isomer.

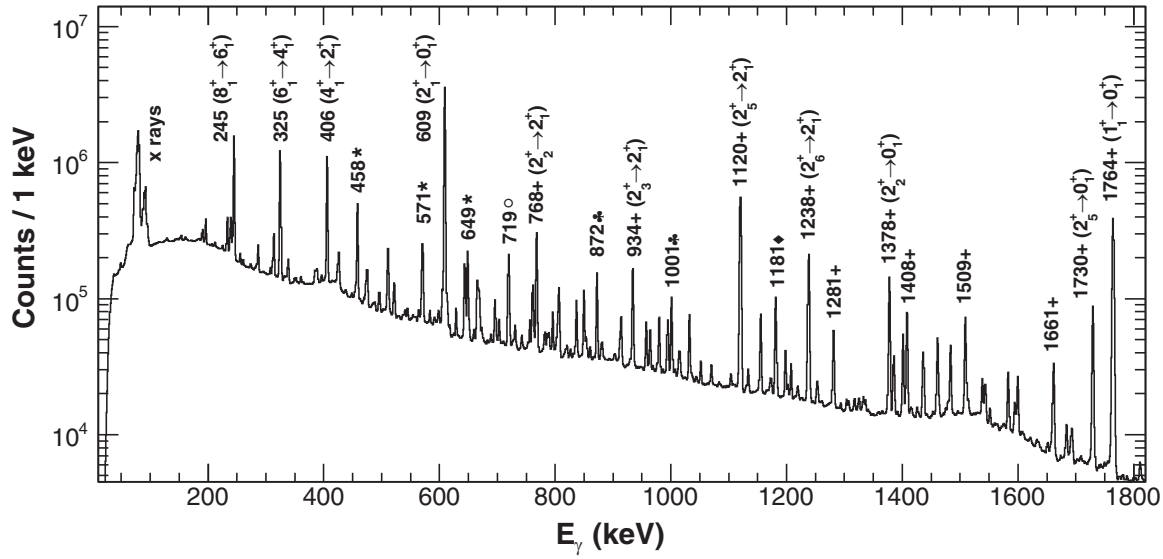


FIG. 1. Singles $\gamma$-ray spectrum. Peaks without a special symbol in the label belong to transitions following the $\beta^-$ decay of $^{214}$Bi$^m$, with the exception of the 406- and 609-keV peaks, which follow the $\beta^-$ decay of both $^{214}$Bi$^m$ and $^{214}$Bi$^g$. The remaining peaks are attributed to the following decays: (+) $\beta^-$ decay of $^{214}$Bi$^g$, (*) EC/$\beta^+$ decay of $^{210}$Rn, (♣) EC/$\beta^+$ decay of $^{205}$Po, (♦) EC/$\beta^+$ decay of $^{210}$At, and (○) EC/$\beta^+$ decay of $^{205}$At.

the $8_1^+$ state (including the 609-keV $\gamma$ ray) will be collectively referred to as "g.s. band transitions" in the following text.

Apart from these g.s. band transitions and $\gamma$-ray peaks following the $\beta^-$ decays of $^{214}$Bi$^g$, transitions following electron-capture and $\beta^+$ (EC/$\beta^+$) decays of $^{210}$Rn, $^{210}$At [1], $^{205}$At, and $^{205}$Po [20] are visible in Fig. 1. The nuclides $^{210}$Rn and $^{210}$At are present in the decay chain of $^{214}$Ra, which is an isobaric contaminant in the beam decaying into $^{210}$Rn with almost 100% $\alpha$-decay branching ratio [1]. Based on the number of counts in the 458-keV peak in Fig. 1 (corrected for absolute $\gamma$-ray intensity from Ref. [1] and efficiency), $8(2) \times 10^8$ nuclei of $^{210}$Rn decayed in the chamber. Isotopes $^{205}$At and $^{205}$Po are members of the decay chain of $^{209}$Fr, which was implanted in the chamber during previous measurements. Transitions of interest were distinguished from the contaminants using $\gamma$-$\gamma$ coincidences (Secs. III A and III B).

It has to be noted that the 245-keV peak in Fig. 1 also contains 245-keV $\gamma$ rays following the EC/$\beta^+$ decays of $^{210}$At [1], while the $4^+$ level in $^{214}$Po, decaying via the 406-keV transition, is very weakly populated also after the $\beta^-$ decay of $^{214}$Bi$^g$ from higher-lying levels [8]. Nevertheless, the comparable intensities of the 245-, 325- and 406-keV peaks in Fig. 1 indicate that they originate mostly from the cascade following the decay of the $8_1^+$ level in $^{214}$Po. The presence of these transitions shows that the $\beta^-$ decay of $^{214}$Bi has to feed to the $8_1^+$ and/or other higher-lying high-spin levels. This proves the existence of a high-spin $\beta^-$-decaying state in $^{214}$Bi ($^{214}$Bi$^m$), since the $\beta^-$ decay of the $1^-$ state cannot populate high-spin levels in $^{214}$Po.

We note that, for the 609- and 406-keV transitions in $^{214}$Po, which were observed both after the $\beta^-$ decay of $^{214}$Bi$^g$ [8] and in the in-beam study [12], the energies given in Ref. [8] are ≈0.3 keV higher compared with Ref. [12]. Similarly, for all $\gamma$-ray transitions (with the exception of the 503-keV line) observed both in our work and in Ref. [12], our energies are systematically 0.2–0.4 keV higher. The typical $\gamma$-ray energy uncertainty was stated to be 0.1–0.5 keV in Ref. [12].

### A. $\gamma$-$\gamma$ coincidences with the ground-state band transitions

Figure 3 shows the $\gamma$-$\gamma$ coincidence spectra gated with the g.s. band transitions below the $8_1^+$ level in $^{214}$Po, for events within a time window of $|\Delta t(\gamma\text{-}\gamma)| < 200$ ns. The 240-keV line is in coincidence with all the g.s. band transitions [Figs. 3(a)–3(d)], which is consistent with its placement as the $8_2^+ \rightarrow 8_1^+$ transition as suggested in Ref. [12]. The weak 575-keV $\gamma$ ray is seen in coincidence with g.s. band transitions between the $8_1^+$ and $2_1^+$ levels [Figs. 3(a)–3(c)], which is also consistent with Ref. [12], where it was assigned as the $9 \rightarrow 8_1^+$ transition (Fig. 2). In the coincidence spectrum of the 609-keV ($2_1^+ \rightarrow 0_1^+$) $\gamma$ ray [Fig. 3(d)], the 575-keV peak is not resolved due to the higher level of background and the partial overlap with the 572.77(7)-keV transition following the $\beta^-$ decay of $^{214}$Bi$^g$ [8].

Additionally, we identified new $\gamma$ rays in coincidence with all g.s. band transitions [Figs. 3(a)–3(d)], which places them above the $8_1^+$ state in the decay scheme (Fig. 2). Their energies are 49.1, 335.5, 384.7, 426.1, 475.1, 564.0, 613.2, and 741.9 keV.

The 613-keV peak is resolved only in Fig. 3(d), because of the proximity to the much stronger 609-keV peak in the other panels [Figs. 3(a)–3(c)]. However, fitting the structure around the 609-keV peak with two Gaussian functions in Fig. 3(b) allowed the energy and intensity of the 613-keV transition to be extracted.

According to NDS [8], two $\gamma$-ray transitions, at the 426.5(5) keV (unplaced in the decay scheme) and at the 474.43(5) keV are reported in the $\beta^-$ decay of $^{214}$Bi$^g$. However, these transitions are different from the 426- and 475-keV

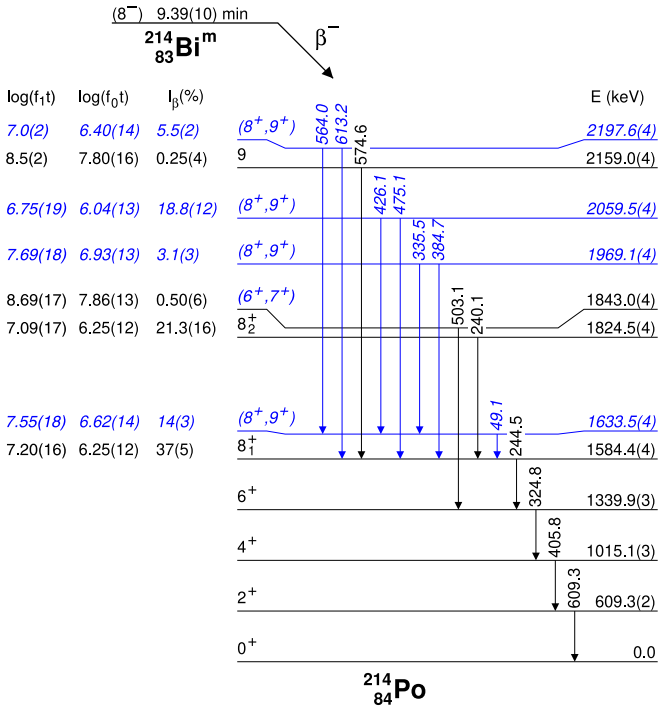


FIG. 2. The decay scheme with levels in $^{214}$Po populated by the $\beta^-$ decay of $^{214}$Bi$^m$. Transitions, levels, and spin and parity assignments written in blue italics are from the present study, while those in black normal font were reported in Refs. [8,12]. For display purposes, the spacing of the g.s. band levels is compressed and not scaled according to their energies. Level energies are deduced from $\gamma$-ray energies listed in Table I. In the case of parallel decay paths from the level, the path with the smaller number of $\gamma$-ray transitions was used. As a result of the systematic shift in energy calibration, discussed in Sec. III, there may be a difference of up to 2 keV in the level energies compared with Ref. [12]. Apparent $\beta$-decay feeding intensities and resulting $\log(f_0t)$, $\log(f_1t)$ values are included, see details in Sec. III E.

$\gamma$ rays shown in Fig. 3, since the new transitions have to be depopulating high-spin levels, as mentioned above.

Finally, a weak 503.1-keV $\gamma$ ray is seen in coincidence with all transitions decaying from the $6_1^+$ state [Figs. 3(b)–3(d)], while there are no coincidences with the $8_1^+ \rightarrow 6_1^+$ transition [Fig. 3(a)]. This pattern is consistent with the 503-keV $\gamma$ ray feeding the $6_1^+$ level observed in Ref. [12].

There seem to be self-coincidences of gating transitions in Figs. 3(a)–3(d). The 245-keV peak in Fig. 3(a) is caused by a small overlap of the energy gate with the 240-keV $\gamma$ ray, which is in coincidence with the 245-keV transition (Fig. 2). The weak, broad structures close to 325 keV in Fig. 3(b) and 406 keV in Fig. 3(c) stem from polonium $K_{\alpha 1}$ x rays ($E$ = 79.3 keV [21]) summed with the 245- and 325-keV transitions, respectively. The 609-keV peak in Fig. 3(d) comes from the two sources. First, there is a small overlap of the energy gate with the 613-keV $\gamma$ ray. Second, the $\gamma$-$\gamma$-$\gamma$ coincidences with the requirement of two $\approx$609-keV $\gamma$ rays revealed coincidences with the 665-, 720- and 1385-keV transitions known from the $\beta^-$ decay of $^{214}$Bi$^g$ [8]. They depopulate the 1995-keV $I^\pi = 1^-$ state in $^{214}$Po [8]. The latter state can be populated from the 2605-keV $I^\pi = (2^+)$ level [8] by a 610-keV transition, which was not observed so far, giving rise to the 610-1385-609-keV and 610-720-665-609-keV cascades. For simplicity, these levels populated in the $\beta^-$ decay of $^{214}$Bi$^g$ are not shown in Fig. 2.

To test the prompt character of the newly identified $\gamma$-ray transitions, $\beta$-$\gamma$ coincidences were used. All of these transitions have prompt coincidences with $\Delta t(\beta\text{-}\gamma) < 200$ ns, which limits their possible multipolarities to $E1$, $M1$, or $E2$. The prompt character of the 613-keV $\gamma$ ray, largely hidden by the 609-keV peak, was confirmed by time differences of 609-613-keV $\gamma$-$\gamma$ coincidences.

The list of $\gamma$-ray transitions following the $\beta^-$ decay of $^{214}$Bi$^m$ is given in Table I and the list of summing peaks present in Fig. 3 is shown in Table II. To calculate transition intensities $I_t$, three approaches to obtain the total internal-conversion coefficients $\alpha_{\rm tot}$ were used and they are noted in the last column of Table I. Experimental values of $\alpha_{\rm tot}$ were used for the 49- and 240-keV transitions. For transitions with known $E2$ multipolarity, the corresponding $\alpha_{\rm tot,th}$ were taken from Ref. [22] and "$E2$" is noted. For transitions with unknown multipolarities, a range of $\alpha_{\rm tot}$ was used. The range was calculated as the average of lower [$\alpha_{\rm tot,th}(E1)$] and upper [$\alpha_{\rm tot,th}(M1)$] limit from Ref. [22], with the uncertainty taken as the difference between the upper and the lower limit divided by two.

Apart from the 609-keV ($2_1^+ \rightarrow 0_1^+$) transition, which is used to normalize the reported intensities, no other transitions feeding the g.s. were observed. Since only the high-spin levels are directly fed in the $\beta^-$ decay of $^{214}$Bi$^m$, the intensities $I_t$ in Table I are directly equal to the absolute transition intensities per 100$\beta^-$ decays of $^{214}$Bi$^m$. To obtain absolute $\gamma$-ray intensities per 100$\beta^-$ decays from $I_\gamma$, the latter needs to be multiplied by a factor $1/[1 + \alpha_{\rm tot}(609\ {\rm keV})] = 0.9800(3)$, where $\alpha_{\rm tot,th}(609\ {\rm keV}, E2) = 0.0204(3)$ [22] was used.

### B. $\gamma$-$\gamma$ coincidences with transitions above ground-state band

Figure 4 presents coincidences with transitions from excited states above the $8_1^+$ level in $^{214}$Po. The 426-keV $\gamma$ ray [Fig. 4(a)] is, apart from the g.s. band transitions, only in coincidence with the 49-keV $\gamma$ ray. Similarly the 49-keV transition [Fig. 4(b)] is only in coincidence with the 426-keV $\gamma$ ray and the cascade below the $8_1^+$ level, which establishes a cascade of 426-49-keV $\gamma$ rays decaying to the $8_1^+$ level. The energy sum of the cascade is 49.1(2) + 426.1(2) keV = 475.2(3) keV which suggests that the 475.1(2)-keV $\gamma$ ray identified in Sec. III A is a crossover transition. Together with the fact that the 475-keV transition is only in coincidence with the g.s. band transitions up to the $8_1^+$ level [Fig. 4(c)] it establishes a new level at 2059.5(4) keV (Fig. 2). We note that a few $\gamma$-ray transitions following the EC/$\beta^+$ decay of $^{210}$Rn are visible in Fig. 4(c). This is caused by the partial overlap of the energy gate with the 472.80(7)-keV $\gamma$ ray from the EC/$\beta^+$ decay of $^{210}$Rn [1].

The intensity of the 426-keV $\gamma$ ray in Fig. 4(b) is apparently much weaker (note the logarithmic scale of the $Y$ axis) compared with g.s. band transitions. The conversion coefficient for any possible multipolarity is small at 426 keV,

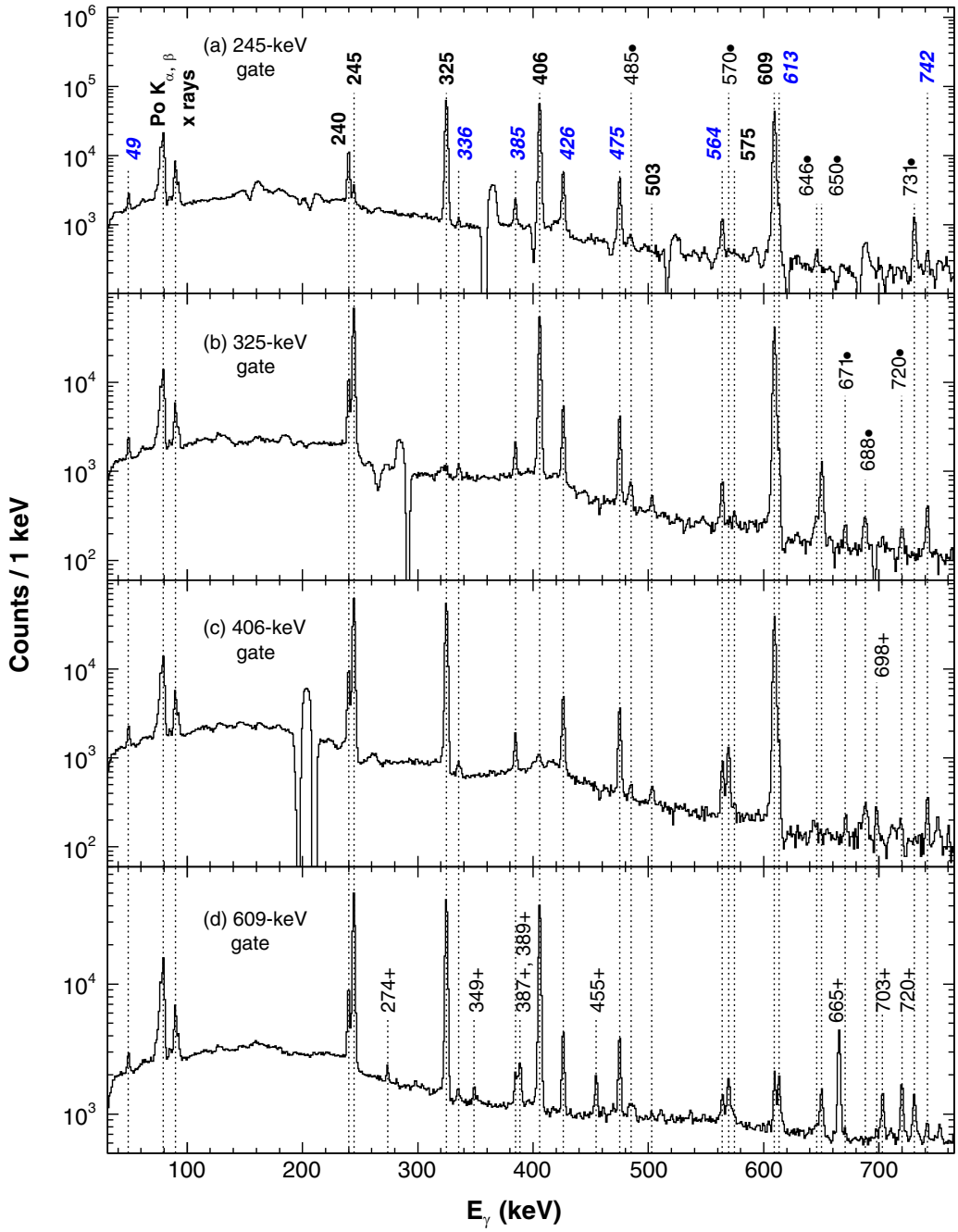


FIG. 3. Background-subtracted spectra of $\gamma$ rays in coincidence with the following g.s. band transitions: (a) 245 keV ($8_1^+ \rightarrow 6_1^+$), (b) 325 keV ($6_1^+ \rightarrow 4_1^+$), (c) 406 keV ($4_1^+ \rightarrow 2_1^+$), and (d) 609 keV ($2_1^+ \rightarrow 0_1^+$). Peaks labeled only by energies belong to transitions following the $\beta^-$ decay of $^{214}$Bi$^m$, transitions with labels in blue italic are new. Peaks marked by bullets are caused by summing of transitions in cascades (the list of these peaks and the relevant cascades are given in Table II), peaks marked by plus signs belong to transitions following the $\beta^-$ decay of $^{214}$Bi$^g$ [8]. The broader peak-like structures with depressions in the background around them are artificial peaks caused by Compton scattering.

so if the gating 49-keV $\gamma$ ray was the first in the 426-49-keV cascade, the 426-keV transition would have to have the same intensity as the subsequent g.s. band transitions. Therefore, the 426-keV $\gamma$ ray has to be the first in the cascade and we establish a 1633.5(4)-keV level decaying via the 49-keV transition to the $8_1^+$ state (Fig. 2). Conversely, the low intensity of the 49-keV peak compared with the g.s. band transitions in Fig. 4(a) is caused by the high conversion coefficient of this low-energy transition, which is further discussed in Sec. III C.

The 240-keV $\gamma$ ray is only in coincidence with the g.s. band transitions [Fig. 4(d)]. Particularly, no coincidences with the 49-keV $\gamma$ ray were observed. The relative $\gamma$-ray intensity $I_\gamma$ of the 240-keV transition is higher than $I_\gamma$ of the 426-keV transition (Table I), for which strong coincidence with the 49-keV $\gamma$ ray was identified [Figs. 4(a) and 4(b)]. Thus, the

TABLE I. $\gamma$-ray transitions following the $\beta^-$ decay of $^{214}$Bi$^m$. $E_\gamma$ stands for $\gamma$-ray energy, $E_i$ and $E_f$ are the respective energies of the initial and the final level of the $\gamma$-ray transition, $I_\gamma$ is the $\gamma$-ray intensity relative to the intensity of the 609-keV $\gamma$ rays, and $I_t$ is the transition intensity relative to the intensity of the 609-keV transition. The energy and intensity for the 325-keV transition are deduced from $\gamma$-$\gamma$ coincidences gated on the 245-keV $\gamma$ ray [Fig. 3(a)], while for the rest, the values are from $\gamma$-$\gamma$ coincidences gated on the 325-keV $\gamma$ ray [Fig. 3(b)]. Total internal-conversion coefficients used to calculate $I_t$ are in the column labeled $\alpha_{\rm tot}$ and the last column notes different approaches to obtain or estimate $\alpha_{\rm tot}$, see text for details. The uncertainty in the $\gamma$-ray energy calibration is 0.2 keV, statistical uncertainties are negligible.

| $E_\gamma$ (keV) | $E_i$ (keV) | $E_f$ (keV) | $I_\gamma$ (%) | $I_t$ (%) | $\alpha_{\rm tot}$ | Note |
|---|---|---|---|---|---|---|
| 49.1 | 1633.5 | 1584.4 | 1.22(9) | 26(3) | 20.6(17) | This work |
| 240.1 | 1824.5 | 1584.4 | 12.8(6) | 21.3(16) | 0.7(1) | [12] |
| 244.5 | 1584.4 | 1339.9 | 83(4) | 101(4) | 0.239(4) | $E2$ |
| 324.8 | 1339.9 | 1015.1 | 95(4) | 102(4) | 0.0999(14) | $E2$ |
| 335.5 | 1969.1 | 1633.5 | 0.59(6) | 0.70(12) | 0.20(17) | $M1$-$E1$ |
| 384.7 | 1969.1 | 1584.4 | 2.18(12) | 2.4(3) | 0.14(12) | $M1$-$E1$ |
| 405.8 | 1015.1 | 609.3 | 97(4) | 100(4) | 0.0542(8) | $E2$ |
| 426.1 | 2059.5 | 1633.5 | 9.5(4) | 10.2(10) | 0.11(9) | $M1$-$E1$ |
| 475.1 | 2059.5 | 1584.4 | 8.1(4) | 8.6(7) | 0.08(7) | $M1$-$E1$ |
| 503.1 | 1843.0 | 1339.9 | 0.47(6) | 0.50(6) | 0.07(6) | $M1$-$E1$ |
| 564.0 | 2197.6 | 1633.5 | 1.31(7) | 1.35(9) | 0.05(4) | $M1$-$E1$ |
| 574.6 | 2159.0 | 1584.4 | 0.24(4) | 0.25(4) | 0.05(4) | $M1$-$E1$ |
| 609.3 | 609.3 | 0 | 100 | 100 | 0.0204(3) | $E2$ |
| 613.2 | 2197.6 | 1584.4 | 4.04(19) | 4.1(2) | 0.04(3) | $M1$-$E1$ |
| 741.9 | | | 0.92(6) | 0.92(6) | 0.025(20) | $M1$-$E1$ |

placement of the 240-keV transition as feeding directly the $8^+_1$ state (Fig. 2) suggested in Ref. [12] is confirmed.

There is also a ≈564-keV peak visible in Fig. 4(d), but it cannot be the 564-keV transition identified in Sec. III A because its intensity is too low.[2] Instead, it belongs to a broader structure caused by Compton scattering of the 804-keV $\gamma$ rays from the EC/$\beta^+$ decay of $^{210}$Rn and 806-keV $\gamma$ rays from the $\beta^-$ decay of $^{214}$Bi$^g$ [8]. Transitions following the EC/$\beta^+$ decay of $^{210}$Rn are visible in Fig. 4(d) because of the overlap between the energy gate and the 238.1(1)-keV transition from the EC/$\beta^+$ decay of $^{210}$Rn [1].

Due to the high conversion coefficient of the 49-keV transition (see Sec. III C), it is not possible to confirm or rule out its coincidences with a number of weaker transitions (336, 385, 564, 613, and 742 keV). However, the energy of the 384.7(2)-keV $\gamma$ ray fits the energy sum of 335.5(2) + 49.1(2) keV, thus we propose a 1969.1(4)-keV level decaying via the 385-keV transition to the 1584-keV state and via the 336-keV $\gamma$ ray to the 1634-keV state. Similarly, the energy of the 613.2(2)-keV $\gamma$ ray is equal to the energy sum of 564.0(2) + 49.1(2) keV, therefore we suggest a 2197.6(4)-keV level decaying via the 613- and 564-keV transitions into the 1584- and 1634-keV states, respectively (Fig. 2). The 564-49-keV cascade is also supported by a hint of the 564-keV peak in the 49-keV gate in the $\gamma$-$\gamma$ coincidences [Fig. 4(b)]. The remaining 742-keV transition may be feeding either the 1584- or the 1634-keV level.

### C. Multipolarity of the 49-keV transition

The total internal-conversion coefficient $\alpha_{\rm tot,exp}$ of the 49-keV transition, depopulating the 1634-keV level, was determined from the spectrum gated by the 426-keV $\gamma$ ray [Fig. 4(a)]. As the 426-keV transition is feeding into the 1634-keV level (Fig. 2), the 49-keV and the subsequent transitions have to have the same intensity after correction for conversion and efficiency within the 426-keV gate [Fig. 4(a)]. By comparing the efficiency corrected number of counts in the 49-keV peak with the number of counts in the 325-keV peak corrected for $\alpha_{\rm tot,th}$(325 keV, $E2$) [22] and efficiency, an $\alpha_{\rm tot,exp}$(49 keV) = 20.6(17) was deduced. This value corresponds to a dominant $M1$ multipolarity [$\alpha_{\rm tot,th}$(49 keV, $M1$) = 16.92(24) [22]] with the possibility of a small $E2$ [$\alpha_{\rm tot,th}$(49 keV, $E2$) = 208(3) [22]] and/or $E0$

TABLE II. List of summing peaks present in Figs. 3 and 4 and summed $\gamma$ or x rays forming these peaks.

| $E_{\rm sum}$ (keV) | $E$ of summed $\gamma$ or x rays (keV) |
|---|---|
| 485 | 240 + 245 |
| | 406 + 79 (x rays) |
| 570 | 245 + 325 |
| 646 | 240 + 406 |
| 650 | 245 + 406 |
| 671 | 245 + 426 |
| 688 | 609 + 79 (x rays) |
| 720 | 245 + 475 |
| 731 | 325 + 406 |

[2]If the 564-keV transition was feeding into $8^+_2$ level, the intensity of the ≈564-keV peak in Fig. 4(d) would have to be the same as the intensity within gates on the subsequent transitions. After correction for efficiency and conversion of respective gating transitions, $N$(564 keV) = 9.5(9) × 10$^3$ in the 240-keV gate, while within the 325-keV gate $N$(564 keV) = 2.34(12) × 10$^4$.

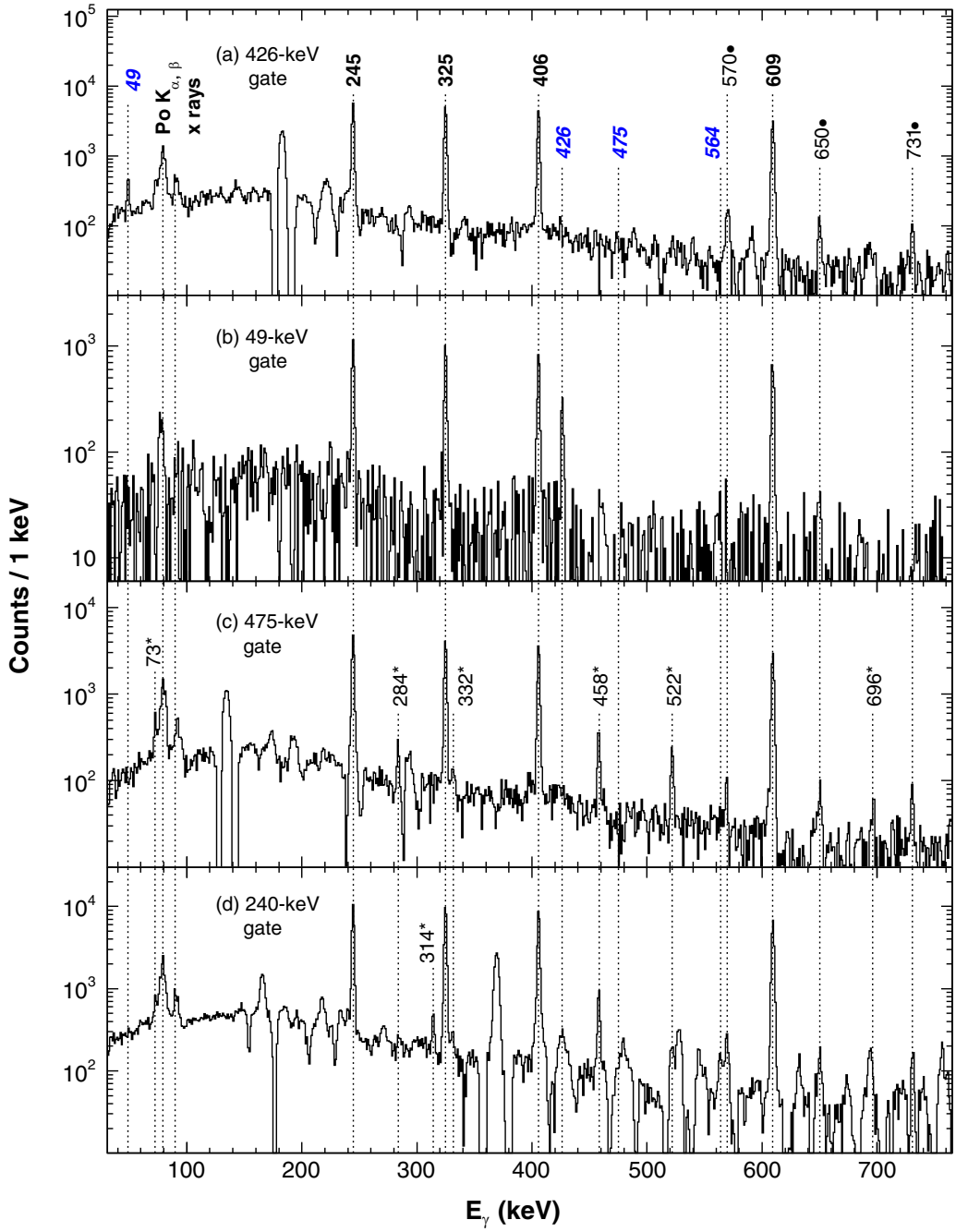


FIG. 4. Background-subtracted spectra of $\gamma$ rays in coincidence with (a) 426 keV, (b) 49 keV, (c) 475 keV, and (d) 240 keV. Peaks labeled only by energies belong to transitions following the $\beta^-$ decay of $^{214}$Bi$^m$, transitions with labels in blue italics are new. Peaks marked by bullets are caused by summing of transitions in cascades (a list of these peaks and relevant cascades is given in Table II), peaks marked by asterisks belong to transitions following the EC/$\beta^+$ decay of $^{210}$Rn [1]. The broader peak-like structures with depressions in the background around them are artificial peaks caused by Compton scattering.

admixture. The possible spin and parity of the 1634-keV level decaying via the 49-keV transition into the $8_1^+$ state can thus be constrained to values $I^\pi = (7^+, 8^+, 9^+)$.

### D. Half-lives of $^{214}$Bi$^m$ and $^{214}$Bi$^g$

A specific experimental setting was used to determine the half-lives of $^{214}$Bi$^m$ and $^{214}$Bi$^g$. After implanting a sample of $A/q = 214$ ions onto the tape, the beam gate was closed and the $\gamma$-ray activity was monitored for about two hours. In the case of $^{214}$Bi$^m$, the intensity variation of the 325-keV transition as a function of time was used to determine its half-life. This $6_1^+ \rightarrow 4_1^+$ transition is not fed in the $\beta^-$ decay of $^{214}$Bi$^g$ and the $\gamma$-$\gamma$ coincidence analysis revealed no contamination of the 325-keV line. The resulting time distribution is shown in Fig. 5(a) and from

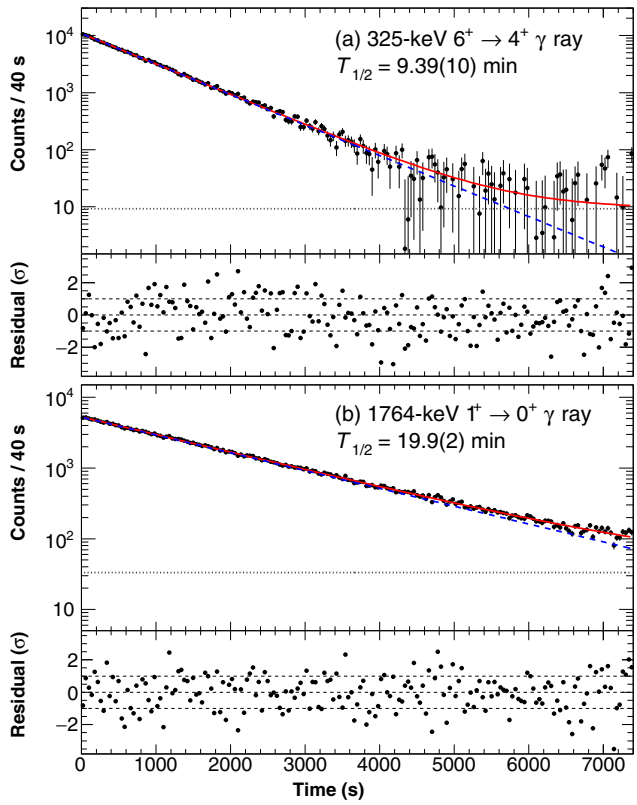


FIG. 5. Background-subtracted time distributions for (a) 325-keV $\gamma$ ray and (b) 1764-keV $\gamma$ ray, obtained when the beam gate was closed. Each distribution was fit (solid red line) by an exponential function (dashed blue line) plus constant (dotted black line). The corresponding normalized residuals of the fits are plotted below each time distribution, dashed lines in these plots mark values of $-1\sigma$, $0\sigma$, and $1\sigma$.

the fit the half-life of $^{214}$Bi$^{m}$ was deduced to be $T_{1/2} = 9.39(10)$ min.

To obtain a clean time distribution of $^{214}$Bi$^{g}$, a gate on the 1764-keV $\gamma$ ray from a relatively high-lying low-spin level (1764 keV $1^+ \rightarrow 0$ keV $0^+$ [8]) was used. The distribution is presented in Fig. 5(b) and yields a $T_{1/2} = 19.9(2)$ min., which is consistent with the literature values of $T_{1/2} = 19.71(2)$ min. [23] and $T_{1/2} = 19.9(4)$ min. [24].

The excellent description of the time distributions in Figs. 5(a) and 5(b) by a single exponential function indicates, that regardless of the relative position of $^{214}$Bi$^{m}$ and $^{214}$Bi$^{g}$ states, there is no strong internal decay between them. Otherwise, the time distribution of the lower-lying level would be distorted by the growth and decay curve caused by internal decays of the higher-lying level. If $^{214}$Bi$^{g}$ were indeed the g.s., the match of the measured $T_{1/2}(^{214}\text{Bi}^{g})$ with the literature values would further support the absence of a strong internal decay branch for $^{214}$Bi$^{m}$.

### E. Spin and parity of $^{214}$Bi$^{m}$

The apparent $\beta$-decay feeding intensities shown in Fig. 2 were estimated as differences between transition intensities depopulating and transition intensities feeding the specific level (the transition intensities are listed in Table I). Using these values, the half-life determined in Sec. III D and the $Q$ value for $\beta$ decay $Q_\beta = 3269(11)$ keV [25], the $\log(ft)$ values were determined by employing the NNDC $\log(ft)$ calculator [26]. Different Fermi integrals need to be used to calculate $\log(f_0 t)$, corresponding to allowed or first forbidden nonunique decays (both types change spin by $\Delta I = 0, 1$), and $\log(f_1 t)$, corresponding to first forbidden unique decays (with $\Delta I = 2$). To distinguish which types of $\beta$ decays are feeding the levels observed in our experiment, both the $\log(f_0 t)$ and the $\log(f_1 t)$ values were calculated and are shown in Fig. 2.

The excitation energy of $^{214}$Bi$^{m}$ needed as an input to $\log(ft)$ calculation is unknown, but based on systematics it is expected to be small. The high-spin [$I^\pi = 9^-$ and $(9^-, 8^-)$] isomers in lighter isotopes $^{210}$Bi and $^{212}$Bi have excitation energies of 271.31(11) keV ($^{210}$Bi$^{m}$) [1] and about 240–250 keV ($^{212}$Bi$^{m}$) [27,28], respectively. In the heavier isotopes $^{218}$Bi, $^{216}$Bi, high-spin g.s. with $I^\pi = (6^-, 7^-, 8^-)$ [4] and $I^\pi = (6^-, 7^-)$ [3,7]), respectively, were proposed. Moreover, a low-spin $I = (3)$ isomer is present in $^{216}$Bi, but because of its low excitation energy with a large uncertainty $E^* = 24(19)$ keV [7], the order of the two long-lived states in $^{216}$Bi is not firmly fixed. Nevertheless, the excitation energy of the high-spin states decreases when going from $^{210}$Bi to $^{218}$Bi and thus it can be assumed that $^{214}$Bi$^{m}$ has an excitation energy below 250 keV. The two shell-model calculations discussed in Sec. IV A are in line with this trend, thus a rounded average of 100 keV from these calculations was used for the excitation energy for the $\log(ft)$ determination. For the latter, the same value of 100 keV was taken as an uncertainty of the excitation energy to cover most of the energy region where the isomer could be expected. Note that using a significantly higher excitation energy of, e.g., 500 keV would only increase the $\log(ft)$ values by ≈0.5-0.6 and the conclusions drawn below would not be altered.

As it is not possible to rule out the presence of a Pandemonium effect [29], the quoted apparent $\beta$-decay feedings have to be considered as upper limits and the $\log(ft)$ values as lower limits. However, the feeding of the $8^+_1$ and $8^+_2$ levels is so strong [37(5)% and 21.3(16)%, respectively], that even if we assume the real direct $\beta$-decay feeding to be only 1/2 of the values from Fig. 2, the resulting $\log(f_1 t)$ values are still well below the $\log(f_1 t) > 8.5$ limit for the first forbidden unique decays [30,31]: 7.50(16) for the $8^+_1$ level and 7.39(17) for the $8^+_2$ state. Thus, the $\log(f_1 t)$ and $\log(f_0 t)$ values for the feeding of the $8^+_1$ and $8^+_2$ levels are consistent only with the first forbidden nonunique or allowed decays with $\Delta I = 0, 1$ [30,31]. Considering, that only negative-parity states are predicted at low excitation energies (<500 keV) for $^{214}$Bi (see Sec. IV A), the decays can be further limited to first forbidden nonunique type and the spin and parity assignments for $^{214}$Bi$^{m}$ can be constrained to $I^\pi = (7^-, 8^-, 9^-)$.

No evidence of direct feeding of the 1340-keV $6^+$ state was found: when gating in $\gamma$-$\gamma$ coincidences on the 325-keV $6^+ \rightarrow 4^+ \gamma$ ray, the transition intensities of the 245-keV $8^+_1 \rightarrow 6^+$, the 406-keV $4^+ \rightarrow 2^+$ and the 609-keV $2^+ \rightarrow 0^+$ transitions are the same within the uncertainties (Table I). If there was a strong direct feeding of the $6^+$ level, it would

cause higher transition intensities of the 406- and 609-keV $\gamma$ rays compared with the 245-keV $\gamma$ ray within this gate [Fig. 3(b)]. Moreover, no feeding of the $10^+$ states reported in Ref. [12] was observed and only a weak feeding of one of the two $I = 9$ states from Ref. [12] was found (Fig. 2). Although the possibility of $I^\pi = (7^-, 9^-)$ for $^{214}$Bi$^m$ cannot be strictly excluded, based on this $\beta$-decay feeding pattern and based on the comparison with shell-model calculations in Sec. IV A, we propose $I^\pi = (8^-)$ as a preferred assignment. This assignment is consistent with the neighboring isotope $^{212}$Bi, where an $I^\pi = (9^-, 8^-)$ isomer is present [2] and for which $I^\pi = 8^-$ was suggested based on comparison of experimental data with shell-model calculations and predicted $\beta$-decay rates [32].

We note, that an isomer in $^{214}$Bi with an excitation energy of 539(30) keV and a half-life of >93 s was identified in Ref. [33]. This isomer was suggested to have $I^\pi = 8^-$ in the NUBASE evaluation [34] based on the trend in neighboring nuclei. Although it is not possible to directly confirm or disprove if $^{214}$Bi$^m$ discussed in the present work is the same state as the one identified in Ref. [33], the trend in excitation energies of isomers and ground-state $I^\pi$ assignments for $^{210\text{–}218}$Bi discussed above, and the shell-model calculations presented in Sec. IV A strongly indicate that such high excitation energy could not correspond to $^{214}$Bi$^m$ identified in our study. Following this conclusion, the isomer from Ref. [33] cannot be explained as an $I^\pi = 8^-$ isomer analogous to isomers in $^{210}$Bi and $^{212}$Bi.

### F. Constraints on spins for levels in $^{214}$Po

Log($f_1t$) values from $\beta$-decay feeding of all newly identified levels in $^{214}$Po (Fig. 2), ranging from 6.8 to 7.7, exclude the possibility of first forbidden unique decays ($\Delta I = 2$) [30,31]. Therefore, we assume that these $\beta$ decays correspond to first forbidden nonunique or allowed decays ($\Delta I = 0, 1$). Considering the preferred $I^\pi = (8^-)$ for $^{214}$Bi$^m$, the possible spins of populated states then range from 7 to 9. As only positive-parity states with these spins are expected below 2.5 MeV (see Sec. IV B), the possible assignments are constrained to $I^\pi = (7^+, 8^+, 9^+)$.

The $I^\pi = (7^+)$ assignments for the new levels can be ruled out by investigating expected $\gamma$-ray intensities for unobserved $M1$ transitions from these levels to the $6^+$ state (Fig. 2). Internal conversion is not taken into account, because corrections for conversion would cancel out in the end when evaluating the hindrances. For example, the 49-keV $M1$ transition from the state at 1634 keV would compete with the 294-keV $M1$ transition feeding the $6^+$ level. Assuming that both transitions had the same reduced $M1$ transition probability $B(M1)$, the ratio of their $\gamma$-ray intensities depopulating the 1634-keV level would be $I_{\gamma,\mathrm{rel,th}}(294\ \mathrm{keV})/I_{\gamma,\mathrm{rel,th}}(49\ \mathrm{keV}) = 214$. Using the measured $\gamma$-ray intensity of the 49-keV transition from Table I to scale $I_{\gamma,\mathrm{rel,th}}(294\ \mathrm{keV})$, the estimated $\gamma$-ray intensity of the 294-keV transition would be $I_{\gamma,\mathrm{th}} = 261\%$. However, the experimental limit of $I_{\gamma,\mathrm{exp}} < 0.20\%$ was determined for the unobserved 294-keV $\gamma$ ray, which means that this transition would have to be hindered by a factor of 1300 (Table III) compared with the $B(M1)$ of the 49-keV transition.

TABLE III. Hindrance of unobserved $M1$ transitions from new levels in $^{214}$Po to the $6^+$ state based on theoretical intensities, see text for details. $E_\gamma$ stands for the energy of unobserved $\gamma$ ray, $E_i$ is the energy of initial level, $I_{\gamma,\mathrm{th}}$ is estimated $\gamma$-ray intensity relative to $I_\gamma$ (609 keV) and $I_{\gamma,\mathrm{exp}}$ is the experimental limit of $\gamma$-ray intensity relative to $I_\gamma$ (609 keV).

| $E_\gamma$ (keV) | $E_i$ (keV) | $I_{\gamma,\mathrm{th}}$ (%) | $I_{\gamma,\mathrm{exp}}$ (%) | Hindrance |
|---|---|---|---|---|
| 293.6 | 1633.5 | 261 | <0.20 | 1304 |
| 629.2 | 1969.1 | 9.5 | <0.13 | 73 |
| 719.6 | 2059.5 | 28.1 | <0.20 | 141 |
| 857.7 | 2197.6 | 11.1 | <0.14 | 79 |

The same procedure was used for parallel observed and unobserved $M1$ transitions to the $8^+_1$ and $6^+$ states from the rest of the new levels at 1969, 2060, and 2198 keV (Fig. 2), assuming their $7^+$ character. The resulting hindrances are shown in Table III. All of the unobserved $M1$ transitions would have to be hindered by a factor of 70 or higher, and therefore the $I^\pi = (7^+)$ assignment is unlikely for all of the levels in Table III.

A log($f_1t$) value of 8.69(17) for the $\beta$-decay feeding of the 1843-keV level (Fig. 2) is above the limit for first forbidden unique decays [log($f_1t$) > 8.5 [30,31]], thus this type of decay cannot be excluded. The 1843-keV level could then have an $I^\pi = 6^+$-$10^+$. However, the specific decay pattern of the level (only the 503-keV transition to the $6^+$ state is observed), gives further constraints on the spin for this state. An $I^\pi = 7^+$ assignment is consistent with the nonobservation of the $M1$ transition to the $8^+_1$ state, because of the lower energy of such transition ($E_\gamma = 259$ keV). Similarly, an $I^\pi = 6^+$ option agrees with the nonobservation of the 259-keV $\gamma$ ray and the 828-keV transition to the $4^+_1$ level, because they would have $E2$ characters and could not compete with the 503-keV $M1$ transition. This conclusion follows from Weisskopf estimates [21], assuming the same $B$ values of 1 W.u. for these transitions. Even the higher energy 828-keV $E2$ $\gamma$ ray, to compete with the 503-keV $M1$ transition (having 50% : 50% relative intensities), $B(E2, 828\ \mathrm{keV})$ would have to be enhanced ≈120× compared with $B(M1, 503\ \mathrm{keV})$. For an $I^\pi = 8^+$ assignment, the 259-keV $M1$ transition to the $8^+_1$ state would be dominant compared with the 503-keV $E2$ $\gamma$ ray to the $6^+$ state, based on Weisskopf estimates assuming the same $B$ values of 1 W.u. for both transitions. To compete with the 259-keV $M1$ transition, the $B(E2, 503\ \mathrm{keV})$ would have to be enhanced ≈300× compared with the $B(M1, 259\ \mathrm{keV})$ value. Finally, the assignments of $9^+$ or $10^+$ for the 1843-keV level would lead to an unrealistic $M3$ or $E4$ character, respectively, for the 503-keV $\gamma$ ray. Therefore, the $I^\pi = (6^+, 7^+)$ assignment is suggested for this level.

## IV. COMPARISON WITH THEORY

### A. Levels in $^{214}$Bi

To get a deeper insight in the nature of $^{214}$Bi$^m$ and of the populated states in $^{214}$Po, shell-model (SM) calculations using two different effective interactions were performed and

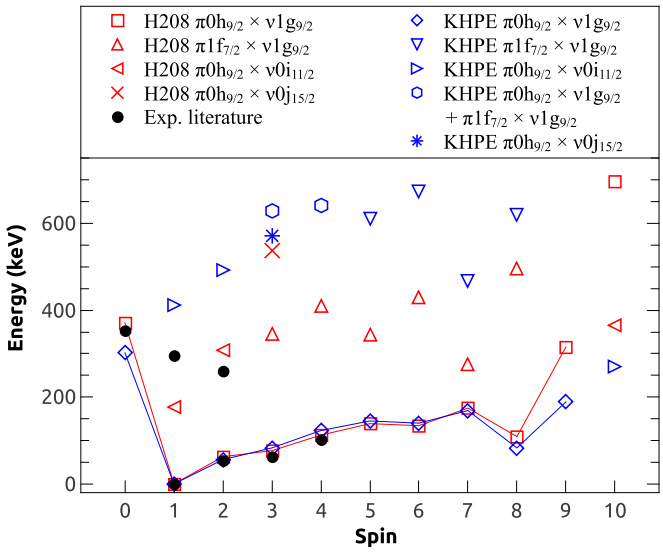


FIG. 6. The calculated energies of yrast and yrare states below 700 keV in $^{214}$Bi using KHPE (blue symbols) and H208 (red symbols) interactions are shown together with the experimental energies (black circles) from Refs. [10,11]. Yrast SM states stemming from the $\pi 0h_{9/2} \otimes \nu 1g_{9/2}$ multiplet are connected by solid lines. Labels indicate dominant configurations of the odd proton and odd neutron.

compared with our measurements. Both calculations used the large particle model space spanning across $0h_{9/2}$, $1f_{7/2}$, $1f_{5/2}$, $2p_{3/2}$, $2p_{1/2}$, $0i_{13/2}$ orbits for protons, and $1g_{9/2}$, $0i_{11/2}$, $1g_{7/2}$, $2d_{5/2}$, $2d_{3/2}$, $3s_{1/2}$, $0j_{15/2}$ orbits for neutrons, lying energetically above the Fermi surface of the $^{208}$Pb closed core.

One of the SM calculations was based on the well-known modified Kuo-Herling particle interaction (KHPE) [35] and employed the SM code KSHELL [36]. The other SM calculation used the new H208 effective interaction [37,38], which was derived by way of many-body perturbation theory of the effective Hamiltonian at second-order of the $Q$-box folded-diagrams [39], starting from a low-momentum two-body potential derived from the CD-Bonn potential [40]. Some adjustments of the monopole component have been fine-tuned to reproduce the proton and neutron single-particle energies of the $N = 126$ and 127 isotonic chains, respectively. The diagonalization of the Hamiltonian of the nuclei of interest was carried out using the ANTOINE SM code [41,42].

Results for yrast and yrare (the second lowest-lying level with a given spin) states in $^{214}$Bi with excitation energies below 700 keV are presented in Fig. 6, along with experimental levels from Refs. [10,11]. In the used model space, $^{214}$Bi is described by one valence proton and five valence neutrons, although mostly the odd proton and odd neutron determine the dominant SM configurations based on the multiplets of proton-neutron matrix elements. The yrast states from $0^-$ to $9^-$ have a dominant $\pi 0h_{9/2} \otimes \nu 1g_{9/2}$ configuration. On average, three neutrons are located in the $1g_{9/2}$ orbital, while the remaining pair is scattered to higher-lying orbitals such as $0i_{11/2}$, $0j_{15/2}$ or sometimes $1g_{7/2}$. The remaining states include configurations with the odd proton or neutron occupying other orbitals such as $\pi 0h_{9/2} \otimes \nu 0i_{11/2}$, $\pi 1f_{7/2} \otimes \nu 1g_{9/2}$, and well-mixed $\pi 0h_{9/2} \otimes \nu 1g_{9/2} + \pi 1f_{7/2} \otimes \nu 1g_{9/2}$. The two SM calculations predict the same first positive-parity state ($3^+$) with a configuration of $\pi 0h_{9/2} \otimes \nu 0j_{15/2}$ at 572 keV (KHPE) and 538 keV (H208), all the other states in Fig. 6 have negative parities.

For the yrast states, there is a good agreement between the calculations and available experimental energies. In the case of yrare states, there is ≈200 keV shift in energies from the two calculations (Fig. 6). Both calculations support $I^\pi = 1^-$ g.s., while higher-spin yrast states roughly follow a flattened downward concave parabola up to $I^\pi = 8^-$ level, which results in the prediction of an $I^\pi = 8^-$ isomeric state with an excitation energy of 83 keV (KHPE) and 109 keV (H208).

The observed parabolic trend in level energies from proton-neutron multiplets in odd-odd nuclei is a well-known phenomenon discussed in Ref. [43], where also an analytic expression for calculation of these level energies was introduced. The latter approach was applied in Ref. [3], assuming the case of pure $\pi 0h_{9/2} \otimes \nu 1g_{9/2}$ multiplets in the heavy bismuth isotopes. Downward concave parabolas of the excitation energy versus spin for $^{210,212}$Bi supported the particle-particle character of the $\pi 0h_{9/2} \otimes \nu 1g_{9/2}$ multiplet, which was to a large extent consistent with the $I^\pi = 1^-$ g.s. and $I = 9^-, (8^-, 9^-)$ isomers in $^{210,212}$Bi. For $^{214}$Bi, a monotone increase of level energies with increasing spin was predicted [3], pointing to a transition towards the proton particle-neutron hole nature of the multiplet. However, the known energies for yrast states from $I^\pi = 1^-$ to $I^\pi = 4^-$, the observation of the $\beta$-decaying isomeric state [$I^\pi = (8^-)$] and the large-scale SM calculations (Fig. 6) suggest that the multiplet appears to partially retain its particle-particle character also in $^{214}$Bi. This follows from the delayed filling of the $\nu 1g_{9/2}$ orbital predicted by the SM calculations, which is caused by the scattering of neutron pairs to higher-lying orbitals mentioned above. Furthermore, the effect of mixing with states belonging to the proton-neutron multiplet $\pi 0h_{9/2} \otimes \nu 0i_{11/2}$ ($I^\pi$ from $1^-$ to $10^-$), and to lesser extent $\pi 1f_{7/2} \otimes \nu 1g_{9/2}$ ($I^\pi$ from $1^-$ to $8^-$) and others, additionally modifies the simple picture of one multiplet.

The results of SM calculations are in agreement with the $\beta$-decay feeding pattern observed for $^{214}$Bi$^m$ in our experiment (Sec. III E) and with the $I^\pi = 1^-$ assignment for $^{214}$Bi$^g$ from the literature [8]. They also fit into the trend of decreasing excitation energies with increasing neutron number observed for the low-lying isomers in $^{210,212,216}$Be [1,2,7] (discussed in Sec. III E). Moreover, both calculations are consistent with the experimental nonobservation of an internal decay branch between $^{214}$Bi$^m$ and $^{214}$Bi$^g$ (see Sec. III D) as the spin gap for the internal decay of the $8^-$ state is $\Delta I \geqslant 4$ with an energy difference of a few dozens of keV.

### B. Levels in $^{214}$Po

Shell-model calculations were also performed for levels in $^{214}$Po using the two SM approaches introduced in Sec. IV A. The calculated level energies are compared with the experimental results in Fig. 7. To simplify Fig. 7 and to focus the discussion on the higher-spin states, observed in the present work, only a limited number of states is displayed. For spins below $I = 6$, only $0^+_1$, $2^+_1$, $4^+_1$ are included, while for $I =$

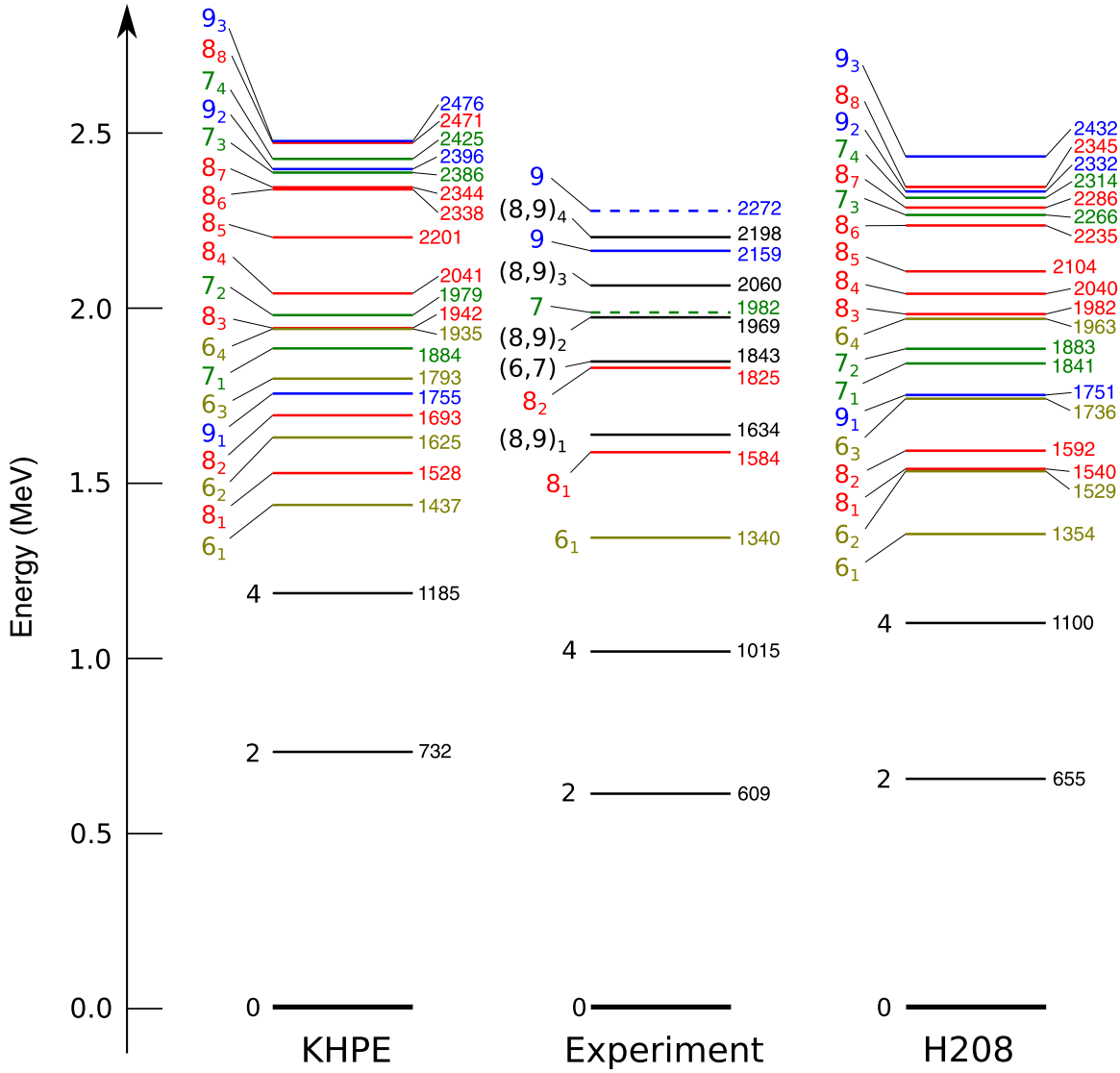


FIG. 7. Comparison of levels in $^{214}$Po from experiment and from SM calculations based on KHPE and H208 interactions. Experimental levels drawn by solid lines are from the present work, with two additional levels with spin 7 and 9 taken from Ref. [12] and drawn as dashed lines. From SM calculations, only levels with spins and energies relevant for comparison with the current experiment are displayed (see Sec. IV B). All of these SM levels have positive parities. Spins are given on the left sides of the levels, energies in keV are given on the right sides. Levels with the same spins are highlighted in the same colors.

6, the four lowest-lying levels are presented. In the case of higher-spin levels with $I = 7, 8, 9$, all SM states below 2.5 MeV are shown. All of the calculated levels within this spin and energy range have positive parities.

The two calculations are in a good agreement with each other, although a systematic shift of up to 50–100 keV to higher energies is observed for the most of the states from the KHPE calculation compared with the H208. We use the calculated energies to guide the identification of the experimentally observed levels in this work. In the following text, the levels from the SM calculations will be denoted by the abbreviation SM and corresponding $I^\pi$ value, for example SM $8^+_1$ state. When discussing consistency of experimental levels with specific SM states, the states from both calculations are considered at the same time if not stated otherwise.

Overall, the agreement between theory and experiment for the members of the g.s. band $(0^+_1, 2^+_1, 4^+_1, 6^+_1, 8^+_1)$ is very good. The next experimental level at 1634 keV, with $I^\pi = (8^+, 9^+)_1$, is close in energy to the SM $8^+_2$ state. However, given the range of spins, the SM $9^+_1$ level ≈120 keV higher might be another possible interpretation for the $(8^+, 9^+)_1$ state. The experimental $8^+_2$ state lies in between the SM $8^+_2$ and SM $8^+_3$ states, thus there is no clear preference to which of the two states it corresponds, unless the SM $8^+_2$ were already assigned to the aforementioned $(8^+, 9^+)_1$ level.

The state at 1843 keV with a proposed $I^\pi = (6^+, 7^+)$ assignment (Fig. 2) is in excellent agreement with the SM $7^+_1$ state (within ≈40 keV). At the same time, this $I^\pi = (6^+, 7^+)$ level lies between the SM $6^+_3$ and SM $6^+_4$ states. Although the energy differences between the experimental state and these $6^+$ levels are somewhat larger (mainly in H208 with

$\Delta E > 100$ keV), the interpretation of the $I^\pi = (6^+, 7^+)$ level as the SM $6_3^+$ or SM $6_4^+$ state cannot be excluded. The $I = 7$ level at 1982 keV from Ref. [12] agrees within 3 keV with the SM $7_2^+$ state from KHPE. Despite almost ≈100 keV discrepancy with the SM $7_2^+$ from the H208, the SM $7_2^+$ state remains to be the most plausible interpretation of this experimental level considering its spin assignment.

In spite of the larger energy difference of up to 150–250 keV, the two $I = 9$ states at 2159 (Fig. 2) and 2272 keV [12] can be associated only with the SM $9_2^+$ and $9_3^+$ states (Fig. 7). It is worth noting that, although the SM level energies are shifted to higher values, the energy differences between the SM $9_2^+$ and $9_3^+$ levels of ≈100 keV (H208) and ≈80 keV (KHPE) are consistent with the difference of ≈110 keV for the two experimental $I = 9$ states.

The three remaining experimental states at 1969, 2060, and 2198 keV with $I^\pi = (8^+, 9^+)$ identified in the present study (Fig. 2) can then be explained as $8^+$ states from the group of the SM $8_3^+$-$8_7^+$ levels (Fig. 7). There is a particularly good agreement in energies of the $(8^+, 9^+)_2$ level with the SM $8_3^+$ state and the $(8^+, 9^+)_3$ level with the SM $8_4^+$ state. However, if the SM $8_3^+$ state would be associated with the experimental $8_2^+$ state, as discussed above, then these $(8^+, 9^+)_2$-$(8^+, 9^+)_4$ levels would be from the group of the SM $8_4^+$-$8_7^+$ levels.

## V. CONCLUSIONS

The new $\beta$-decaying state in $^{214}$Bi (denoted $^{214}$Bi$^m$) and populated states in $^{214}$Po have been studied at the ISOLDE Decay Station. Based on the observed $\beta$-decay feeding pattern to states in $^{214}$Po, deduced lower limits of $\log(ft)$ values and comparison with shell-model (SM) calculations, a spin-parity assignment of $I^\pi = (8^-)$ was proposed for $^{214}$Bi$^m$. A half-life of $T_{1/2} = 9.39(10)$ min. was measured for $^{214}$Bi$^m$, while for the previously known $I^\pi = 1^-$ $\beta$-decaying state in $^{214}$Bi ($^{214}$Bi$^g$) a half-life of $T_{1/2} = 19.9(2)$ min. was deduced, which agrees with previous value of $T_{1/2} = 19.71(2)$ min. [23].

The decays of excited states populated in $^{214}$Po via the $\beta$ decay of $^{214}$Bi$^m$ were investigated using $\gamma$-$\gamma$ coincidences. Several new levels and $\gamma$-ray transitions were identified and placed into the decay scheme. Possible spins of the new levels were proposed based on deduced $\log(ft)$ values and comparison of the observed deexcitation pattern with theoretical $\gamma$-ray intensities for depopulation of the states.

Experimental results were compared with two different SM calculations for excited states in $^{214}$Bi and $^{214}$Po based on the H208 interaction [37,38] and the modified Kuo-Herling particle interaction (KHPE) [35]. Both SM calculations interpret $^{214}$Bi$^m$ as an $I^\pi = 8^-$ isomer and $^{214}$Bi$^g$ ($I^\pi = 1^-$) as the ground state. Tentative assignments of SM states from the calculations to several high-spin states in $^{214}$Po were possible. Namely, the three highest-lying $(8^+, 9^+)$ states from the present work may be interpreted as $8^+$ states from the group of the shell-model $8_3^+$-$8_7^+$ levels, and the experimental $I = 9$ levels reported in Ref. [12] can be associated with the shell-model $9_2^+$, $9_3^+$ states, respectively.

## ACKNOWLEDGMENTS

We thank the ISOLDE Collaboration for providing excellent beams and the GSI Target Group for manufacturing the carbon foils. This work has been supported by the Research Foundation Flanders (FWO, Belgium), by GOA/2015/010 (BOF KU Leuven), the Interuniversity Attraction Poles Programme initiated by the Belgian Science Policy Office (BriX network P7/12), by the ENSAR2: European Union's Horizon 2020 research and innovation programme under Grant Agreement No. 654002, by the U.K. Science and Technology Facilities Council, by the Slovak Research and Development Agency (Contract No. APVV-18-0268), by the Slovak grant agency VEGA (Contract No. 1/0651/21), by RFBR according to the research project N 19-02-00005, by the Romanian IFA Grant CERN/ISOLDE, by the Spanish Funding Agency (AEI) under the project PID2019-104390GB-I00, by the German BMBF under Grant No. 05P18PKCIA and by the Spanish Ministerio de Ciencia e Innovación grant PID2019-104714GB-C21. M.S. acknowledges funding from the European Union's Horizon 2020 research and innovation program under Grant Agreement No. 771036 (ERC CoG MAIDEN).

[1] M. Shamsuzzoha Basunia, Nucl. Data Sheets **121**, 561 (2014).
[2] K. Auranen and E. A. McCutchan, Nucl. Data Sheets **168**, 117 (2020).
[3] J. Kurpeta, A. Andreyev, J. Äystö, A.-H. Evensen, M. Huhta, M. Huyse, A. Jokinen, M. Karny, E. Kugler, J. Lettry *et al.*, Eur. Phys. J. A **7**, 49 (2000).
[4] H. De Witte, A. N. Andreyev, I. N. Borzov, E. Caurier, J. Cederkäll, A. De Smet, S. Eeckhaudt, D. V. Fedorov, V. N. Fedosseev, S. Franchoo, M. Górska, H. Grawe, G. Huber, M. Huyse, Z. Janas, U. Köster, W. Kurcewicz, J. Kurpeta, A. Płochocki, K. Van de Vel, P. Van Duppen, and L. Weissman, Phys. Rev. C **69**, 044305 (2004).
[5] D. G. Burke, H. Folger, H. Gabelmann, E. Hagebø, P. Hill, P. Hoff, O. Jonsson, N. Kaffrell, W. Kurcewicz, G. Løvhøiden *et al.*, Z. Phys. A **333**, 131 (1989).
[6] E. Ruchowska, J. Zylicz, C. F. Liang, P. Paris, and C. Briançon, J. Phys. G **16**, 255 (1990).
[7] S.-C. Wu, Nucl. Data Sheets **108**, 1057 (2007).
[8] S. Zhu and E. A. Mccutchan, Nucl. Data Sheets **175**, 1 (2021).
[9] G. Mouze, O. Diallo, P. Bechlitch, J. F. Comanducci, and C. Ythier, Radiochim. Acta **49**, 13 (1990).
[10] Z. Berant, R. B. Schuhmann, D. E. Alburger, W. T. Chou, R. L. Gill, E. K. Warburton, and C. Wesselborg, Phys. Rev. C **43**, 1639 (1991).
[11] J. G. Cubiss, A. N. Andreyev, A. E. Barzakh, B. Andel, S. Antalic, T. E. Cocolios, T. D. Goodacre, D. V. Fedorov, V. N. Fedosseev, R. Ferrer, D. A. Fink, L. P. Gaffney, L. Ghys, M. Huyse, Z. Kalaninová, U. Köster, B. A. Marsh, P. L. Molkanov, R. E. Rossel, S. Rothe, M. D. Seliverstov, S. Sels, A. M. Sjödin,

M. Stryjczyk, V. L. Truesdale, C. Van Beveren, P. Van Duppen, and G. L. Wilson, Phys. Rev. C **99**, 064317 (2019).
[12] A. Astier and M.-G. Porquet, Phys. Rev. C **83**, 014311 (2011).
[13] R. Catherall, W. Andreazza, M. Breitenfeldt, A. Dorsival, G. J. Focker, T. P. Gharsa, T. J. Giles, J.-L. Grenard, F. Locci, P. Martins *et al.*, J. Phys. G **44**, 094002 (2017).
[14] E. Kugler, Hyperfine Interact. **129**, 23 (2000).
[15] V. Fedosseev, K. Chrysalidis, T. Day Goodacre, B. Marsh, S. Rothe, C. Seiffert, and K. Wendt, J. Phys. G **44**, 084006 (2017).
[16] V. N. Fedoseyev, G. Huber, U. Köster, J. Lettry, V. I. Mishin, H. Ravn, V. Sebastian, and the ISOLDE Collaboration, Hyperfine Interact. **127**, 409 (2000).
[17] S. Rothe, T. Day Goodacre, D. V. Fedorov, V. N. Fedosseev, B. A. Marsh, P. L. Molkanov, R. E. Rossel, M. D. Seliverstov, M. Veinhard, and K. D. A. Wendt, Nucl. Instrum. Methods Phys. Res., Sect. B **376**, 91 (2016).
[18] A. N. Andreyev, A. E. Barzakh, N. Althubiti, B. Andel, S. Antalic, J. Billowes, M. Bissell, K. Chrysalidis, T. E. Cocolios, J. Cubiss *et al.*, Addendum to the IS608 Proposal to the ISOLDE and Neutron Time-of-Flight Committee, https://cds.cern.ch/record/2241202?ln=en (2017).
[19] ISOLDE Decay Station, https://isolde-ids.web.cern.ch/.
[20] F. G. Kondev, Nucl. Data Sheets **101**, 521 (2004).
[21] R. B. Firestone *et al.*, *Table of Isotopes*, CD-ROM Edition (John Wiley & Sons, New York, 1996).
[22] T. Kibédi, T. W. Burrows, M. B. Trzhaskovskaya, P. M. Davidson, and C. W. Nestor Jr., Nucl. Instrum. Methods Phys. Res., Sect. A **589**, 202 (2008).
[23] D. E. Martz, G. H. Langner, and P. R. Johnson, Health Phys. **61**, 511 (1991).
[24] H. Daniel and R. Nierhaus, Z. Naturforsch. A **11**, 212 (1956).
[25] M. Wang, W. J. Huang, F. G. Kondev, G. Audi, and S. Naimi, Chin. Phys. C **45**, 030003 (2021).
[26] NNDC log($ft$) calculator, https://www.nndc.bnl.gov/logft/.
[27] P. A. Baisden, R. E. Leber, M. Nurmia, J. M. Nitschke, M. Michel, and A. Ghiorso, Phys. Rev. Lett. **41**, 738 (1978).
[28] L. Chen, P. M. Walker, H. Geissel, Y. A. Litvinov, K. Beckert, P. Beller, F. Bosch, D. Boutin, L. Caceres, J. J. Carroll, D. M. Cullen, I. J. Cullen, B. Franzke, J. Gerl, M. Górska, G. A. Jones, A. Kishada, R. Knöbel, C. Kozhuharov, J. Kurcewicz, S. A. Litvinov *et al.*, Phys. Rev. Lett. **110**, 122502 (2013).
[29] J. C. Hardy, L. C. Carraz, B. Jonson, and P. G. Hansen, Phys. Lett. B **71**, 307 (1977).
[30] S. Raman and M. B. Gove, Phys. Rev. C **7**, 1995 (1973).
[31] B. Singh, J. L. Rodriguez, S. S. M. Wong, and J. K. Tuli, Nucl. Data Sheets **84**, 487 (1998).
[32] E. K. Warburton, Phys. Rev. C **44**, 261 (1991).
[33] L. Chen, PhD Thesis, Justus-Liebig University Gießen, Germany, 2008 (unpublished).
[34] F. G. Kondev, M. Wang, W. J. Huang, S. Naimi, and G. Audi, Chin. Phys. C **45**, 030001 (2021).
[35] E. K. Warburton and B. A. Brown, Phys. Rev. C **43**, 602 (1991).
[36] N. Shimizu, T. Mizusaki, Y. Utsuno, and Y. Tsunoda, Comput. Phys. Commun. **244**, 372 (2019).
[37] H. Naïdja, Phys. Scr. **94**, 014005 (2019).
[38] H. Naïdja, Phys. Rev. C **103**, 054303 (2021).
[39] M. Hjorth-Jensen, T. T. S. Kuo, and E. Osnes, Phys. Rep. **261**, 125 (1995).
[40] R. Machleidt, Phys. Rev. C **63**, 024001 (2001).
[41] E. Caurier and F. Nowacki, Acta Phys. Pol. B **30**, 705 (1999).
[42] E. Caurier, G. Martínez-Pinedo, F. Nowack, A. Poves, and A. P. Zuker, Rev. Mod. Phys. **77**, 427 (2005).
[43] V. Paar, Nucl. Phys. A **331**, 16 (1979).